## RESEARCH ARTICLE

# The Analysis of Nutrition Toxicology Detection Based on Big Data and Deep Learning

**JING SHI[1,2], RENJUAN CHEN[2], YONGHONG MA[1,3], YANCHENG FENG[1,3], AND KE MEN[1,3]**

[1]Institute for Research on Health Information and Technology, Xi'an Medical University, Xi'an, Shaanxi 710021, China
[2]Department of Nutrition Hygiene and Toxicology, Xi'an Medical University, Xi'an 710021, China
[3]Research Center for Medical Prevention and Control of Public Safety of Shaanxi Province, Xi'an 710021, China

Corresponding author: Ke Men (menke@xiyi.edu.cn)

**ABSTRACT** Public health and safety are increasingly concerned as public awareness of health-related issues grows. To find a rapid, convenient, and non-destructive testing method for detecting human nutritional toxicology detection, this study selects sildenafil, phenolphthalein, and metformin hydrochloride—commonly found additives in health products—as the focal point. The research endeavors to tackle the paramount issue of public health and safety. The study begins by elucidating the public health and safety concept and then outlines the computational process for determining the terahertz (THz) optical properties. Subsequently, it provides a brief overview of deep learning (DL) methods, including the Back Propagation Neural Network (BPNN), Convolutional Neural Network (CNN), Residual Network (ResNet), and MobileNet model. Finally, the study compares and tests the THz absorption spectrum data of 22 pure samples containing sildenafil, phenolphthalein, and metformin hydrochloride by DL technique to evaluate the model's classification performance. The findings demonstrate that, with increased training iterations, the model's accuracy consistently improves and stabilizes. For instance, after 12 training iterations, CNN's accuracy under the verification set stabilizes, frequently reaching nearly 100%. After 83 iterations, the accuracy remains steady at 98.96%. Similarly, the MobileNet model reaches stability after 17 iterations, achieving 100% accuracy. The BPNN demonstrates the fastest prediction time among the four DL algorithm models, at 310-5 seconds. Meanwhile, the MobileNet model exhibits the highest accuracy and stability. This study using THz waves to identify contaminants in medical items can significantly enhance public health and safety.

**INDEX TERMS** Public health and safety, additives in health products, deep learning, BP neural network, terahertz wave.

## I. INTRODUCTION

As public awareness regarding health continues to expand, public health and safety concerns have gained increasing prominence. Information is omnipresent in the modern age of information proliferation, from the Internet to social media. This trend undeniably has positive aspects as it facilitates easier access to health information and awareness, ultimately promoting healthier lifestyles. However, it also brings novel challenges, notably the proliferation of misinformation and the marketing of health products. Various health products claim to enhance one's quality of life, boost physical well-being, and bolster immunity. Regrettably, some of these may contain potentially harmful ingredients, threatening public health and safety [11].

The motivation for this study is based on the current expansion of the health products market and the intensification of regulatory challenges. The current traditional detection methods often find it difficult to effectively identify potential harmful components in health products, leading to increasing attention to public health and safety. Regulatory and testing tasks have become more complex and urgent with the diver-

The associate editor coordinating the review of this manuscript and approving it for publication was Claudio Loconsole.

sification of health products and increased market demand. This motivation comes from filling the technological gap in this field, intending to provide an innovative, fast, and accurate detection method for safeguarding public health. By combining terahertz (THz) technology and deep learning (DL) method, it is hoped to break the limitations of traditional detection methods, provide efficient and non-destructive testing (NDT) means of health products, and ensure the public's safe consumption of health products. As a scientific discipline, Toxicology studies the effects of toxicants on living organisms and the development of strategies for preventing and mitigating exposure to such harmful substances. Within this domain, prioritizing public health and safety has always been a central concern [40]. Nevertheless, with the expanding market for health products, regulation and detection has evolved into a multifaceted challenge. Frequently, the potentially hazardous components within healthy products elude identification through traditional detection methods, thus necessitating an innovative solution to tackle this issue.

As an advanced NDT method, THz technology boasts the unique capacity to conduct high-spectrum measurements of samples. While this technique has heralded pivotal breakthroughs in medicine, food safety, and materials science [21], its application in nutritional toxicology detection has remained relatively limited. Thus, this study introduces THz technology into this field with the aspiration of fashioning a novel, swift, and efficient detection method to ensure the quality and safety of health products. Furthermore, as a cutting-edge technology in artificial intelligence (AI), DL has achieved remarkable feats across diverse fields, including image recognition, natural language processing, and medical image analysis [22]. Kumari and her colleagues have proposed a novel process model for IoT-based Multimedia Big Data (MMBD). This process model addresses numerous research challenges associated with MMBD, including scalability, accessibility, reliability, heterogeneity, and quality of service requirements [5]. The study leverages advanced technological approaches to handle and analyze large-scale data and explores how to utilize data in complex environments efficiently. This study examines the feasibility of employing DL to assess the information derived from the THz spectrum of ingredients in health products.

This study aims to develop a DL-based method for nutritional toxicology detection. The purpose is to utilize DL models to analyze and predict the toxicological properties of different chemicals, thereby facilitating a more robust assessment of potential risks in food and cosmetics and enhancing product safety. At the same time, the study also explores techniques based on high-frequency THz to obtain information about the sample's internal structure. It combines this with DL models to enhance the accuracy and efficiency of the detection. Moreover, the study thoroughly examines the THz absorption spectrum data from 22 pure samples containing sildenafil, metformin hydrochloride, and phenolphthalein. The analysis uses the DL method to assess the model's

classification performance. This process facilitates a comprehensive assessment of the benefits and drawbacks of the four algorithms under investigation. In conclusion, this study promotes the incorporation of DL into the field of toxicology to enhance public health and safety.

The outstanding contribution of this study is its fusion of high-frequency THz technology and DL technology to create a new NDT method that can quickly and accurately detect harmful substances in health products. The method can effectively identify and classify potentially harmful substances that may exist, introducing an unprecedented, innovative approach to nutritional toxicology detection. Due to the precise spectral information provided by THz technology and the effective processing of complex spectral data by the DL model, this fusion technology can fully use THz technology's advantages and realize highly accurate toxicology detection through DL technology. In addition, through detailed analysis of THz absorption spectrum data of 22 pure samples containing sildenafil, metformin hydrochloride, and phenolphthalein, this study provides a new research idea and method for the field. It offers more reliable technical support for public health and safety. The innovation of this study is that it leads the development of nutritional toxicology detection and provides a powerful guide and reference for future related research.

## II. LITERATURE REVIEW

Numerous researchers have explored the interconnectedness between the lives and health of the general population. Lake et al. searched five research databases to compile a list of cannabis-related public health and safety issues. They established a set of indicators to evaluate the effects of cannabis legislation in Canada on public health and safety, gauge potential hazards, and weigh the significance of potential benefits amidst emerging topics and themes [34]. Fan et al. scrutinized establishing an authorized environment-operational capability-public value framework by municipal governments to create a safety net for public health and safety, particularly in response to public health emergencies such as the COVID-19 pandemic. They introduced a unique classification of four efficient urban action structures: social guarantee, active defense, decisive flexibility, and enforcement, designed to curb the outbreak's spread [12]. Moyce and Schenker chose migrant workers as their research subjects and probed into the associations between their health, environmental factors, and line of work. Their investigation unveiled that several common factors contributed to the poor health, work-related injuries, and occupational fatalities of migrant workers. These factors included linguistic or cultural barriers, limited access to healthcare, the uncertain status of their immigration documents, and the prevailing political climate of the host nation [32]. Nawaz et al. thoroughly examined the factors influencing the health and safety of nearby inhabitants and primary project stakeholders, concentrating on large-scale infrastructure projects (Orange Line Metro Train). Their research pinpointed several paramount

factors affecting the health and safety of residents. These factors encompassed unsafe working practices, limitations in the project scope, inadequacies in technical and material support, hazardous and challenging working conditions, environmental deterioration affecting public health, depletion of resources and time, an inadequate emergency response system, and negligence in adhering to safety regulations and laws [5]. Boadu et al. examined how the distinctive characteristics of the construction industry in developing countries affect health and safety management within the sector. Their study provided insights into the practical and theoretical impact of the industry's foundation and attributes on health and safety. A questionnaire survey involving professionals in Ghana brought to light the significant challenges in health and safety management in developing nation's construction industry, including a shortage of skilled and educated laborers, a reliance on labor-intensive techniques, and the absence of a single regulatory body [16]. Safonov conducted nutritional and toxicological assessments of the milk quality of black and white Holstein cows. The author revealed that Holstein hybridization positively influenced the concentration of cobalt, zinc, and manganese. Conversely, purebred black and white cows showed the potential for milk contamination by lead and cadmium [44]. Lietzow conducted nutritional and toxicological tests on mustard plant seeds to assess potential health risks. Their findings indicated that consuming mustard seeds or their derived products did not pose immediate health risks for individuals without mustard protein allergies. However, high intake levels of mustard seeds or related products, such as mustard seed oil, raise the possibility of health problems [19].

In the realm of healthcare-oriented fog computing research, Kumari et al. analyzed the role of fog computing, cloud computing, and the Internet of Things (IoT). Their investigation culminated in proposing a three-tier patient-driven healthcare architecture designed for real-time data collection, processing, and transmission. This architecture offers valuable insights to end-users, elucidating the appropriateness of fog devices and gateways in current and future healthcare 4.0 environments [4]. Kumari et al. [5] utilized the characteristics of multimedia big data on the IoT regarding scalability, accessibility, reliability, heterogeneity, and quality of service requirements to process complex multimedia data. Kumari and Tanwar [1] proposed a novel big data analysis scheme that used encryption technologies such as digital signatures to protect data security to deal with security issues such as data modification and integrity attacks. In terms of data analysis and secure transmission, Kumari et al. [3] analyzed the major threats and risks in the processing of large data in the IoT environment, and the security approach required against these risks. Kumari et al. [2] used DL technology to predict energy load and manage energy use according to time priorities, building a Redills system to help users use appliances economically. Tanwar et al. [38] proposed an energy theft detection scheme based on DL

technology that utilized a data-driven analytical approach to identify various forms of energy theft.

In the domain of DL's technical applications in human toxicology detection, Vekaria et al. [15] proposed a bidirectional Long Short-Term Memory (LSTM)-based DL model. This innovative model demonstrated the capability to predict the total number of positive cases in India and evaluate their economic impact. Notably, the model exhibited a remarkably low mean absolute percentage error value of 1.27% and outperformed the most advanced methods in terms of prediction accuracy. Furthermore, Tanwar et al. [39] introduced an AI-based scheme with a cloud-centric disease detection and prevention approach. The results of their research attested to the scheme's impressive prediction accuracy, which reached 96.2%. Zhao et al. [23] emphasized the potential of DL approaches in predicting in vitro, in vivo, and clinical outcomes, thereby advancing drug discovery and development in the era of big data. Rodriguez et al. [37] employed the drug repurposing in Alzheimer's disease (AD) machine learning (ML) framework to explore potential associations between quantifying AD severity and the molecular mechanisms encoded in a list of gene names. Zhao et al. [28] innovatively proposed an end-to-end bioinspired model based on Convolutional Neural Network (CNN) and attention mechanisms to predict drug-target interactions. Their research revealed that this model significantly improved performance in this context. Abbas et al. [20] presented and implemented a new drug supply chain management and recommendation system based on blockchain and ML technologies. The ML module used N-gram and the light Gradient Boosting Machine model to recommend the most highly rated or optimal drugs to customers in the pharmaceutical industry. This enhancement significantly improved drug supply efficiency in this industry. Nag et al. [36] reviewed current challenges and prospects for using DL tools in drug development. They summarized the various DL-based tools available in the public domain and their application in the drug discovery paradigm. Additionally, they highlighted the use of various DL-based models for protein structure prediction, collectively validating the utility of DL tools for pharmaceutical and computational chemists.

The mentioned research investigates public health and safety across various fields and industries, encompassing non-medical marijuana, public health during the COVID-19 epidemic, critical infrastructure, migrant labor, and the construction industry. It underscores the significance of data analysis and the integration of emerging technologies in diverse fields, laying a valuable foundation for the current study. However, there may be some limitations to these studies. For example, in some studies, there may be a lack of comprehensive surveys of specific populations or insufficient consideration of certain potential influencing factors. Moreover, some studies may have data collection or method selection limitations. Most importantly, the application of specific toxicological detection methods in the context of big data and DL has not been fully explored in the existing

literature. This study examines nutrition and toxins in health-care products, which are widely consumed substances closely linked to public health and safety. This study introduces an unprecedented approach to nutritional toxicology detection by melding THz technology with DL. Its novelty and research contribution lies in addressing public health and safety concerns and introducing novel technologies into the field, opening new pathways for swift, precise, and NDT. The amalgamation of THz and DL technology presents substantial potential for practical applications to enhance public health and safety, offering a more efficient tool for health product regulation. Therefore, this study is distinctive and innovative in applying emerging technology and exploring public health issues.

## III. RESEARCH METHODOLOGY

### A. PUBLIC HEALTH AND SAFETY

Individuals experience an enhancement in their material well-being, which fuels an increasing aspiration for more than just sustenance; it fosters a demand for food that satisfies hunger and contributes to overall health and well-being. Consequently, public health has emerged as a prominent topic of concern. The World Health Organization emphasizes that health encompasses a holistic, stable, harmonious condition encompassing physical, psychological, and social dimensions. Health encompasses physical and mental well-being [9]. Public health is a multifaceted issue that demands local, national, and global attention. The memory of the 2013 infant milk powder crisis remains vivid, illustrating the critical importance of ensuring the quality of infant nutrition products. Quality issues related to infant milk powder can inflict irreversible and severe harm on infants and young children, potentially leading to lasting physiological impairments and, in severe cases, significantly affecting their lives. Public health and safety, in this context, diverge from the more commonplace concept of health and safety. The distinct characteristics of public health and safety are displayed in Figure 1.
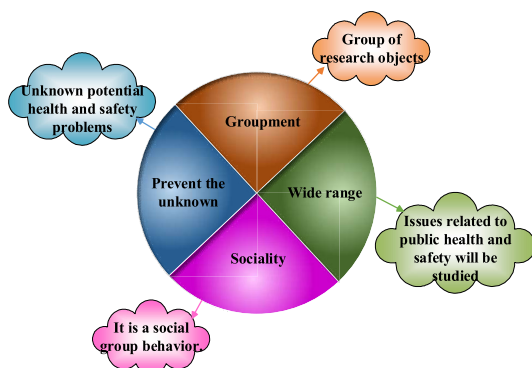


**FIGURE 1.** Unique features of public health and safety.

Figure 1 illustrates four key characteristics of public health safety: collectivity, pre-emptive prevention, comprehensive-

ness, and societal involvement [35]. First, it emphasizes collectivity, focusing on the health issues affecting populations rather than individual health statuses. This underscores the communal nature of the research object. Second, public health safety is associated with pre-emptive prevention, actively addressing potential health and safety concerns before they manifest. Third, it encompasses a wide scope, encompassing a broad spectrum of public health and safety topics, rather than being confined to a single aspect of research. Fourth, public health and safety are inherently social constructs, shaped by societal development and involving the entire community. It is a collective social endeavor. In recent years, public health and safety have covered maternal and child products, health products, epidemic diseases, vaccines, nutrients, and other aspects. This study focuses on the nutritional toxicology of additives in healthcare products, with specific attention to three common additives: sildenafil, phenolphthalein, and metformin hydrochloride. Metformin hydrochloride is used in healthcare products to lower blood sugar and promote weight loss. However, prolonged use can lead to issues like nausea and malnutrition. Phenolphthalein can treat chronic constipation and is included in slimming health products to relieve constipation, but its prolonged consumption can cause permanent damage to intestinal nerves. Sildenafil is added to health products for its stimulating effects and fatigue relief, but prolonged usage can cause cardiovascular damage [6], [29].

### B. CALCULATION OF OPTICAL PARAMETERS OF THz WAVE

THz wave exhibits wave propagation and light penetration characteristics, with a frequency of approximately 1 THz. They offer distinct advantages, such as low energy consumption and exceptional penetration capabilities, making them invaluable for applications in imaging and NDT. Typically, the THz time-domain spectrum captures essential THz information from samples [8]. The analysis of THz spectrum data allows for extracting internal structural characteristics from the samples, facilitating their classification. Analyzing the THz refractive index and absorption spectrum in experimental settings is necessary to discern the sample's characteristics, a process achievable through calculation methods [18], [49]. Assuming that the measured THz signal is denoted as $A_{THz}(\alpha)$ and using the THz signal obtained from spectrum analysis in pure nitrogen as the reference signal $A_{ck}(\alpha)$, the relationship between these signals can be written as equation (1).

$$A_{ck}(\alpha) = A_{THz}(\alpha)e^{-k\tilde{z}(\alpha)M/L} \tag{1}$$

$\tilde{z}(\alpha)$ refers to the complex refractive index, calculated in equation (2).

$$\tilde{z}(\alpha) = z(\alpha) - kc(\alpha) \tag{2}$$

$z(\alpha)$ represents the refractive index, and $c(\alpha)$ signifies the extinction coefficient. These parameters reflect the response of the sample to THz. This study uses a computational model

known as the optical parameter calculation model to calculate the absorption coefficient $W(\alpha)$ of the sample. Equation (2), also called the optical parameter calculation model, facilitates the expression of the absorption coefficient as $\omega(\alpha) = 2\alpha c(\alpha)/L$ [46]. After the sample is placed, the signal obtained by the THz signal passing through the sample is represented as $A_{yp}(\alpha)$. The THz wave is utilized for the sample spectrum. During this process, it undergoes a sequence of refraction and reflection events within the sample. This progression can be articulated as equation (3).

$$QW(\alpha) = \sum \{t_{xy}[e^{-k\tilde{z}_y(\alpha)m/L}]^2 t_{yx}\}^n \tag{3}$$

Here, $\tilde{z}_y(\alpha)$ denotes the complex refractive index of the sample, $m$ signifies the sample's thickness, and $n$ stands for the number of reflections experienced by THz waves in the sample. In practical experiments, the impact of reflection on the experimental results can be mitigated by controlling the sampling frequency. In such cases, it is reasonable to assume that $n = 0$ and $QW(\alpha) = 1$. Consequently, this study can establish the relationship between the sample signal $A_{yp}(\alpha)$ and the reference signal $A_{ck}(\alpha)$, thus allowing for the expression of the sample signal $A_{yp}$ as equation (4).

$$A_{yp}(\alpha) = A_{THz}(\alpha)r_{xy}e^{-k\tilde{z}_y(\alpha)\alpha m/l}r_{yx} \tag{4}$$

In a vacuum, it can be considered that $z = \tilde{z}_y = 1$. This relationship is following equation (5).

$$P(\alpha) = \frac{A_{yp}(\alpha)}{A_{ck}(\alpha)} \tag{5}$$

Equation (6) can be deduced:

$$P(\alpha) = \frac{A_{yp}(\alpha)}{A_{ck}(\alpha)} = \frac{4\tilde{z}_y}{(1+z_y)^2}e^{-k\frac{\alpha m}{L}(\tilde{z}_y-1)} \tag{6}$$

Equations (5) and (6) are used to calculate the absorption rate $\rho(\alpha)$ and phase $\varphi(\alpha)$ of the sample. To derive equations (7) and (8), equation (2) is integrated into equation (6).

$$\rho(\alpha) = \frac{4[z_y^2(\alpha) + c_y^2]^{1/2}}{[z_y(\alpha)+1]^2}e^{-c_y(\alpha)m\alpha/L} \tag{7}$$

$$\varphi(\alpha) = \frac{[z_y(\alpha)-1]\alpha m}{L} + arctg[\frac{c_y(\alpha)}{z_y(\alpha)[z_y(\alpha)+1]+c_y^2(\alpha)}] \tag{8}$$

Therefore, the extinction coefficient $c_y(\alpha)$, refractive index $z_y(\alpha)$, and absorptivity $\omega_y(\alpha)$ of the sample can be obtained as illustrated in equations (9), (10), and (11):

$$c_y(\alpha) = \ln\left\{\frac{4z_y(\alpha)}{\rho(\alpha)[z_y(\alpha)+1]^2}\right\}\frac{L}{\alpha m} \tag{9}$$

$$z_y(\alpha) = \varphi(\alpha)\frac{L}{\alpha m} + 1 \tag{10}$$

$$\omega_y(\alpha) = \frac{2c_y(\alpha)\alpha}{L} = \frac{2}{m}\ln\left\{\frac{4z_y(\alpha)}{\rho(\alpha)[z_y(\alpha)+1]^2}\right\} \tag{11}$$

The above mathematical equations contribute to a more profound comprehension of THz propagation and interaction within the sample. Furthermore, they elucidate the methodology for calculating critical parameters related to toxicological detection.

### C. SIMPLE DL ALGORITHMS

The Back Propagation Neural Network (BPNN) is one of the earliest DL networks. During the training process, it encompasses signals' forward propagation and errors' backward propagation [45]. The hidden BPNN model is depicted in Figure 2 [25].
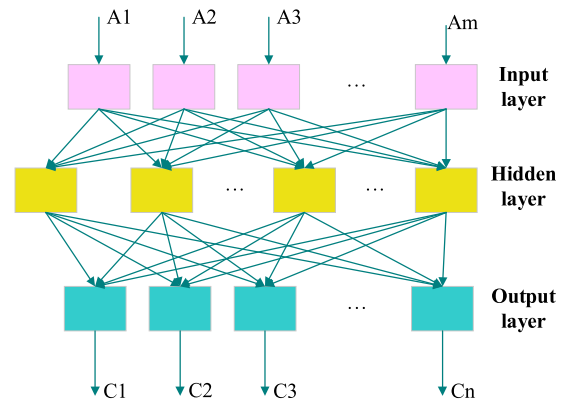
**FIGURE 2.** Three-layer structure of the BPNN with a single hidden layer.

In Figure 2, $A = (a_1, a_2, \cdots, a_u, \cdots, a_m)^T$ is the input vector, the hidden layer vector is $B = (b_1, b_2, \cdots, b_u, \cdots, b_m)^T$, and the output vector is $C = (c_1, c_2, \cdots, c_v, \cdots, c_n)^T$. The output is $D = (d_1, d_2, \cdots, d_v, \cdots, d_n)^T$, the weight matrix from the input layer to the hidden layer is $\omega = (\omega_1, \omega_2, \cdots, \omega_u, \cdots, \omega_m)$, and the weight matrix from the hidden layer to the output layer is $\varphi = (\varphi_1, \varphi_2, \cdots, \varphi_v, \cdots, \varphi_n)$.

$$C_v = f(net_v), \quad v = 1, 2, \cdots, n \tag{12}$$

$$net_v = \sum_{u=0}^{m}\varphi_{iv}b_u, \quad v = 1, 2, \cdots, n \tag{13}$$

$$b_u = f(net_u), \quad u = 1, 2, \cdots, m \tag{14}$$

$$net_u = \sum_{i=0}^{n}\omega_{iu}a_i, \quad u = 1, 2, \cdots, m \tag{15}$$

where f (*) is the transfer function.

$$f(x) = \frac{1}{1+e^{-x}} \tag{16}$$

Within the BPNN framework, the activation function of the input layer is the ReLu, and for the output layer, it is the Softmax. The backpropagation algorithm is responsible for executing the training process of BPNN. Data on chemicals with established toxicological properties are used to train the network. This training data is divided into training and validation sets to facilitate parameter optimization and evaluate network performance. The primary training goal is to minimize the loss function, using the mean square error as the

chosen loss function. Additional techniques, such as random initialization of weights and batch normalization, enhance training stability and network performance.

In CNN, one neuron can correspond with other neurons within its spatial coverage, thus facilitating weight sharing and exceptional processing of a substantial volume of information [14]. CNN significantly reduces the number of learning parameters, thus enhancing the algorithm's performance in training [48]. A typical CNN architecture comprises input, convolutional, pooling, output, and fully connected (FC) processing layers. In the experiment, input data takes the form of chemical structure images. Following the convolution of these input images with specific convolution kernels, the convolutional layer 1 is generated. Then, pixel sampling is performed on each feature map in the convolutional layer 1 to create the pooling layer 1. Further iterations of convolution and sampling yield convolutional layer 3 and pooling layer 4. Moreover, the feature map from pooling layer 4 is transformed into a feature vector through the FC layer and subsequently linked to the output layer. The underlying operational mechanism of the convolutional layer involves convolving the convolution kernel with the feature information from the preceding layer, followed by the addition of an offset term. Finally, the feature information of the new layer is generated by applying a nonlinear activation function [33]. The operation of the convolutional layer reads.

$$q_j^l = f(\sum_{i \in A_j} t_i^{l-1} u_{ij}^l + \varphi_j^l) \qquad (17)$$

$l$ means the number of convolutional layers; $f$ refers to the nonlinear activation function; $q_j^l$ indicates the $j$th feature information in the convolutional layer $l$; $u_{ij}^l$ represents the convolution kernel; $A_j$ is the input feature information set; $\varphi_j^l$ signifies the bias term. After the convolutional layer, the pooling layer is gained. The operational procedure of the pooling layer closely mirrors that of the convolutional layer. In this phase, down-sampling occurs within local regions of the feature information from the upper layer, and this process is as follows [24].

$$w_j^n = f[t_j^l down \left(q_j^{l-1}\right) + \varphi_j^l] \qquad (18)$$

$w_j^n$ refers to the $j$th feature information in the pooling layer $n$; $t_j^l$ means the sampled value; down (*) represents the subsampling function. The FC layer integrates different feature maps extracted by the convolutional layer into a feature vector, which is then input into the classifier for classification. The training code for both BPNN and CNN is exhibited in Table 1. For BPNN, a classical feedforward neural network used in supervised learning tasks, the code first defines the network's structure, including the input, hidden, and output layers. Then, a loss function and an optimizer are specified to facilitate model optimization during training. The training data is iterated to train the model, with weights and biases updated through a backpropagation algorithm to minimize the loss function. Ultimately, the model's performance is evaluated, and performance indicators such as accuracy on

**TABLE 1.** The code of the training part of the BPNN and CNN.

| BPNN | CNN |
|---|---|
| import torch<br>import torch.nn as nn<br>import torch.optim as optim<br><br>class BPNeuralNetwork(nn.Module):<br>def __init__(self, input_size, hidden_size, output_size):<br><br>super(BPNeuralNetwork, self).__init__()<br>self.fc1 = nn.Linear(input_size, hidden_size)<br>self.fc2 = nn.Linear(hidden_size, output_size)<br>self.relu = nn.ReLU()<br>def forward(self, x):<br><br>x = self.fc1(x)<br><br>x = self.relu(x)<br>x = self.fc2(x)<br><br>return x<br>criterion = nn.MSELoss()<br>optimizer = optim.Adam(model.parameters(), lr=0.001)<br>for epoch in range(num_epochs): | class CNNModel(nn.Module):<br>def __init__(self, num_classes):<br>super(CNNModel, self).__init__()<br>self.conv1 = nn.Conv2d(3, 16, kernel_size=3, padding=1)<br><br>self.conv2 = nn.Conv2d(16, 32, kernel_size=3, padding=1)<br><br>self.pool = nn.MaxPool2d(kernel_size=2, stride=2)<br>self.fc1 = nn.Linear(32 * 32 * 32, 128)<br><br>self.fc2 = nn.Linear(128, num_classes)<br><br>def forward(self, x):<br>x = self.pool(nn.functional.relu(self.conv1(x)))<br>x = self.pool(nn.functional.relu(self.conv2(x)))<br>x = x.view(-1, 32 * 32 * 32)<br>x = nn.functional.relu(self.fc1(x))<br>x = self.fc2(x)<br>return x<br>criterion = nn.CrossEntropyLoss()<br><br>optimizer = optim.Adam(model.parameters(), lr=0.001)<br>for epoch in range(num_epochs): |

the validation set are calculated. CNN is a DL model specially designed for processing images and 2D data. The code includes convolutional, pooling, FC, and other layers to extract and learn image features. Network weights are updated by backpropagation to minimize classification errors. Tools such as ImageDataGenerator are also utilized to load and enhance image data.

### D. COMPLEX DL ALGORITHMS

Complex DL algorithms, particularly the Residual Network (ResNet) and MobileNet, are the primary focus of this discussion. In DL, as network model layers increase, the issue of gradient vanishing or explosion arises, impeding network convergence during training and extending training durations. To solve this challenge, scholars have proposed the deep ResNet, which establishes direct connections between certain input information and the output layer to reduce computational load [13]. ResNet incorporates residual connections that facilitate the smoother flow of information throughout the network, thus alleviating the vanishing gradients issue and enhancing overall training feasibility. Incorporating a ResNet significantly augments the model's expressiveness,

a characteristic particularly valuable in complex feature extraction tasks. ResNet has achieved excellent performance in image classification, object detection, and semantic segmentation, making it highly relevant for toxicology detection tasks. The pivotal component within ResNet is the residual unit, as revealed in Figure 3 [42].
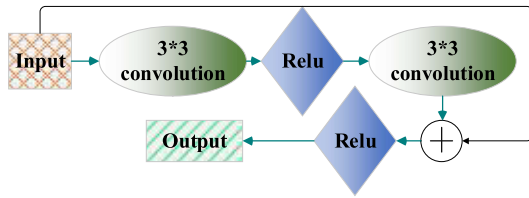


**FIGURE 3.** ResNet structure.

Figure 3 illustrates the journey of the training image through ResNet, encompassing the convolutional layer and the nonlinear activation function layer. A deep ResNet comprises several residual neural units, with the normalization layer ensuring image model normalization. They then undergo computation through multiple residual units, followed by batch normalization and FC layer processing, which converts the results into the expected format to yield the output outputs. Building upon the ResNet architecture, this study introduces a self-attention mechanism and combines feature information from diverse scales. This augmentation allows the network to emphasize crucial regions pertinent to toxicants with images. Besides, feature information of different scales is combined to enhance the network's ability to recognize toxicants and improve detection performance. Additionally, the network incorporates 20 residual blocks to deepen its capacity for capturing intricate image details and features.

MobileNet is designed to operate in resource-constrained environments, making it well-suited for embedded devices and mobile applications. This attribute is pivotal for the swift and easy detection of toxicology. The core idea of MobileNet involves the replacement of traditional convolutions with deep separable convolutions. This substitution mitigates redundant operations in standard convolutional kernels, thereby streamlining model computations [20]. The lightweight and efficient design of MobileNet facilitates fast real-time inference on devices with limited resources, a critical aspect of emergency toxicology detection. Figure 4 highlights the distinctions and transformations between depth separable and standard convolution [26].

Figure 4 illustrates how depth separable convolution divides the standard volume into two components: the depth convolution and the size 1*1 convolution. This method significantly reduces the model's computational workload, allowing for the execution of complex DL algorithms even on resource-constrained systems. In the MobileNet architecture, input data is sequentially processed through the 3*3 depth convolutional layer and the 1*1 pointwise convolutional layer, effectively replacing the standard convolution model
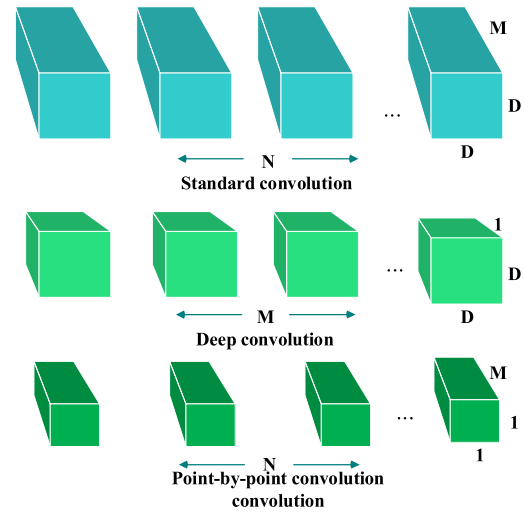


**FIGURE 4.** Conversion of standard convolution to depth separable convolution.

and substantially reducing computational overhead. Furthermore, the MobileNet design incorporates a normalization operation layer and applies the nonlinear activation function ReLu after the deep and pointwise convolutional layers, enhancing the network's computational efficiency. Based on MobileNet, this study introduces a channel attention mechanism and leverages transfer learning. Using pre-trained model weights, the network can adaptively select the most crucial feature channels to expedite model training and enhance overall performance. The training code for both ResNet and MobileNet is outlined in Table 2. ResNet is described as a deep neural network structure in the code, which defines the ResNet model and specifies the appropriate loss functions and optimizers. Training data is applied to train the model, and backpropagation updates the model's weights. Performance evaluations are conducted at the end of each training cycle. TensorFlow, a widely used library, is applied for these purposes. MobileNet is characterized by its lightweight architecture, which is particularly suitable for computationally constrained scenarios. The code includes defining the MobileNet model, compiling, and selecting appropriate loss functions and optimizers. Training data is employed to train the model, and weight updates during each training cycle.

The human nutritional toxicology detection process is suggested in Figure 5.

Figure 5 shows the nutritional toxicology detection process, which commences with preparing and cleaning experimental data. This phase involves sourcing the data, performing data cleaning, and labeling. Subsequently, various DL models (BPNN, CNN, ResNet, MobileNet) are configured, specifying the number and type of layers. The following step exhibits the training process for these models, involving data input, loss function calculation, backpropagation, and weight updates. Finally, the model's performance is evaluated, and its performance results are described, analyzed, and interpreted.

**TABLE 2.** Code for the training part of ResNet and MobileNet.

| ResNet | MobileNet |
|---|---|
| import torch | train_datagen = ImageDataGenerator( |
| import torch.nn as nn | rescale=1.0 / 255, |
| import torch.optim as optim | rotation_range=20, |
| from torchvision import models, transforms, datasets | width_shift_range=0.2, |
| num_epochs = 10 | |
| batch_size = 32 | height_shift_range=0.2, |
| learning_rate = 0.001 | shear_range=0.2, |
| transform = transforms.Compose([ | zoom_range=0.2, |
| transforms.Resize((224, 224)), | horizontal_flip=True, |
| transforms.ToTensor(), | |
| | fill_mode='nearest' |
| transforms.Normalize(mean=[0.485, 0.456, 0.406], std=[0.229, 0.224, 0.225]) | ) |
| ]) | train_generator = train_datagen.flow_from_directory( |
| train_dataset = datasets.ImageFolder('train_data', transform=transform) | 'train_data', target_size=(224, 224), |
| train_loader = torch.utils.data.DataLoader(train_dataset, batch_size=batch_size, shuffle=True) | batch_size=batch_size, |
| model = models.resnet18(pretrained=True) | class_mode='categorical' |
| num_classes = len(train_dataset.classes) | ) |
| model.fc = nn.Linear(model.fc.in_features, num_classes) | base_model = MobileNet(weights='imagenet', include_top=False) |
| criterion = nn.CrossEntropyLoss() | x = base_model.output |
| optimizer = optim.Adam(model.parameters(), lr=learning_rate) | x = GlobalAveragePooling2D()(x) |
| for epoch in range(num_epochs): | x = Dense(1024, activation='relu')(x) |
| for inputs, labels in train_loader: | predictions = Dense(len(train_generator.class_indices), activation='softmax')(x) |
| optimizer.zero_grad() | model = Model(inputs=base_model.input, outputs=predictions) |
| | for layer in base_model.layers: layer.trainable = False |
| outputs = model(inputs) | |
| loss = criterion(outputs, labels) | criterion = tf.keras.losses.CategoricalCrossentropy() |
| loss.backward() | optimizer = Adam(lr=learning_rate) |
| optimizer.step() | model.compile(optimizer=optimizer, loss=criterion, metrics=['accuracy']) |
| print(f'Epoch [{epoch + 1}/{num_epochs}], Loss: {loss.item()}') | model.fit(train_generator, epochs=num_epochs) |
| torch.save(model.state_dict(), 'resnet_model.pth') | |

## IV. EXPERIMENTAL DESIGN AND PERFORMANCE EVALUATION

### A. DATASETS COLLECTION

Traditional toxicology studies typically rely on relatively small datasets and experimental methods. However, larger
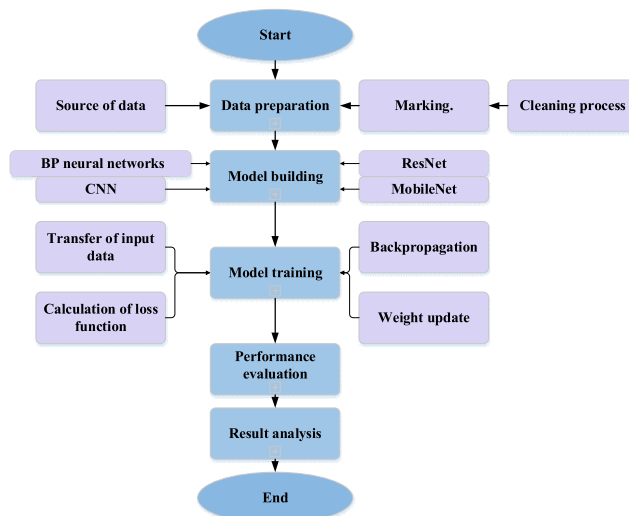
**FIGURE 5.** Human nutritional toxicology detection procedures.

and more diverse datasets are introduced to take advantage of DL technology. Specifically, it utilizes THz absorption spectrum data from 22 pure samples containing sildenafil, phenolphthalein, and metformin hydrochloride. The dataset contains many samples and associated parameters, encompassing nutritional composition and potential toxicity indicators. These data serve as the foundation for training and validating the proposed DL model, enabling more precise detection of potential toxicity in nutraceuticals. The process of obtaining spectral signals from different substances involves several key steps. Initially, the experimental pure samples are ground into powder to ensure sample uniformity and consistency. Subsequently, these powdered samples are mixed with polyethylene in a ratio of 1:1 and formulated into tablets following established standards. This meticulous process guarantees the consistency of the experimental sample. Following the tablet preparation, the samples are subjected to a THz time-domain spectrum device with a 0.2-2 THz frequency. This step is crucial for capturing the THz time-domain spectrum of the samples. Lastly, the obtained THz time-domain data undergo Fourier transformation to yield the frequency domain spectrum of the samples. This transformation enables the calculation of the THz absorption spectrum and refractive index spectrum for each sample, according to the THz optical parameter calculation model. The experiments are conducted in a tightly controlled environment to ensure repeatability and accuracy of the data. The THz time-domain spectrum device is operated under stable laboratory conditions where environmental parameters such as temperature and humidity are monitored and controlled. In addition, to exclude the influence of external factors, the atmosphere in the laboratory is usually filled with pure nitrogen to maintain the consistency of the experimental environment. Multiple data sources in the experiment are used to build this "big data" collection, involving chemical composition data from different food and nutritional products

and known toxicity information. The integration and analysis of these data sources enable a more comprehensive data set to assess the potential toxicity of food and nutritional products. This process covers data cleaning, consolidation, and labeling to ensure quality and availability.

Finally, 234 groups of absorption spectrum data were obtained, averaging approximately 10 sample data points with each group. After meticulous sample preparation, the specimens were introduced into the THz time-domain spectrum device to acquire the THz time-domain spectrum. Subsequently, all data were normalized to obtain a waveform with a size of 224*224 as input for DL classification. These absorption spectra were taken as a training set and testing set in the ratio of 3:2.

## B. EXPERIMENTAL ENVIRONMENT AND PARAMETERS SETTING

During the experiment, a pulsed THz time-domain spectrometer was used as the experimental equipment, and the parameter settings and computer configuration are described in Table 3.

**TABLE 3.** Experimental configuration and parameter setting of THz time-domain spectrometer.

| Processor CPU | Intel(R)Core (TM) i7-7700HQ 2.8GHz |
|---|---|
| Memory | 16GB |
| Operating system | Windows S10 Home Chinese Version |
| Output power | 920mw |
| Wavelength | 810nm |
| Femtosecond laser power | 24nj |

The experimental temperature was maintained at a constant temperature of 25°C with a relative humidity of 2%. The BPNN was assigned a learning rate 0.01 in the model training phase. It featured a hidden layer with 128 neurons, a batch size 64, and 20 training rounds. The learning rate of CNN was set to 0.01, the input size of the input layer was 76*1*1, the number of convolution kernels in the convolutional layer was 16, and the convolution kernel size was 1. The batch size was 32, and the number of training rounds was 15; The learning rate of ResNet training with PyTorch is 0.001, the number of training rounds and the batch size were 10 and 32; The learning rate for MobileNet training with TensorFlow was 0.001, the batch size and the number of training rounds were 32 and 10.

## C. PERFORMANCE EVALUATION

The performance evaluation of the DL method necessitates the utilization of a confusion matrix to show the classification results of the model clearly. Table 4 elaborates on the specifics of the confusion matrix.

In Table 4, the first row refers to the Actual categories (Actual Positive indicates a true example, and Actual

**TABLE 4.** Confusion matrix.

| | Actual Positive | Actual Negative |
|---|---|---|
| Predicted Positive | TP | FP |
| Predicted Negative | FN | TN |

Negative indicates a true negative example). The first column shows the model's prediction (Predicted Positive and Predicted Negative mean that the prediction is positive and negative). TP represents the number of positives that the model correctly predicts the positives to be positive. FP represents the number of negatives that the model incorrectly predicts as positives. TN indicates the number of negatives that the model correctly predicts as negatives. FN refers to the number of positives that the model incorrectly predicts as negatives.

Considering the practical feasibility of the techniques and methods used to integrate a new toxicological detection method with THz technology and DL method, and ensuring that the study can be sustainable and feasible in practical application. The consideration of communication cost can help evaluate the resource consumption in the data transmission process, including the volume of data transmission, the use of communication equipment, and the associated expenses. This helps determine the efficiency and cost-effectiveness of data transfer, ensuring that the data transfer process is efficient, reliable, and cost-effective. Computational cost considerations can help assess the computational complexity of the adopted DL algorithms and techniques as well as the computational resources required. This is conducive to determining the scalability and efficiency of the algorithm, as well as the feasibility and cost-effectiveness of the computing equipment required, guaranteeing that the study enables efficient data processing and analysis in practical applications. The calculation of communication cost and calculation cost is shown in equations (19) and (20):

$$Communication\ cost = V_{data} * C_{nt} \qquad (19)$$

$$Calculated\ cost = T_{run} * C_{nc} \qquad (20)$$

$V_{data}$ represents the data volume; $C_{nt}$ means the unit data transmission cost; $T_{run}$ refers to the running time; $C_{nc}$ is calculated as the unit. The calculation of communication cost first determines the amount of data that needs to be transmitted by analyzing the data size or data volume. The transmission speed, bandwidth, and other parameters of communication equipment used for data transmission are evaluated considering the transmission rate of communication equipment. Second, the time required to complete the data transfer is calculated according to the data volume and the transmission rate. Lastly, the time required for data transmission and the associated use costs of the communication equipment are considered, including the equipment's operating and maintenance costs, to determine

the total communication cost. The calculation costs first require assessing the amount of data processing required, including factors such as the amount of computation to be performed and computational complexity. The performance parameters of the computing equipment used for data processing, such as processing speed and memory capacity, are analyzed. Then, the time required to complete the data processing is calculated according to the amount of data processing and the performance parameters of the computing equipment. Finally, the time required for data processing and the associated cost of using the computing equipment are taken into account, encompassing the operating and maintenance costs of the equipment, to determine the total computing cost.

First, a simple DL model was trained. Due to the limited data samples, training employs the BPNN with a single hidden layer, and the training process is presented in Figure 6.
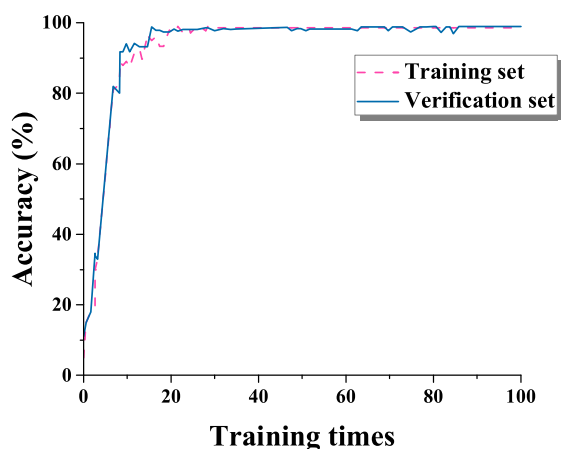


**FIGURE 6.** BPNN model's training process.

Figure 6 denotes that its accuracy constantly improves as the model undergoes more training cycles. Specifically, the model's accuracy under the training set stabilizes at 30 training iterations, ultimately reaching 98.58%. Similarly, the model's accuracy under the validation set stabilizes after 30 iterations and peaks at 98.96% after 87 iterations. The learning and training process of CNN is plotted in Figure 7.

Figure 7 illustrates that as the number of training iterations increases, the accuracy of the CNN model steadily improves. The model's accuracy under the training set stabilizes after about 10 training iterations. Meanwhile, the model's accuracy under the verification set starts to stabilize at 12 after 12 iterations, reaching 100% after numerous iterations and ultimately stabilizing at 98.96% after 83 iterations. The training process of ResNet and MobileNet models is demonstrated in Figure 8.

Figure 8 implies that the MobileNet model begins to stabilize after 12 iterations and reaches complete stability after 17 iterations, with accuracy of 100%. The ResNet model begins to stabilize at 32 iterations, achieves a 100% accuracy after 40 iterations, and maintains 100% accuracy for most of the remaining time, ultimately stabilizing at 100%. The
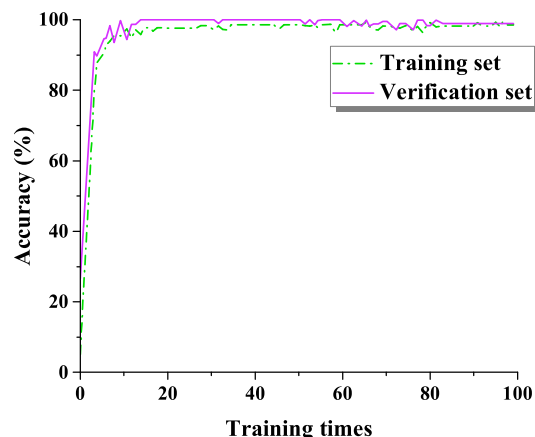


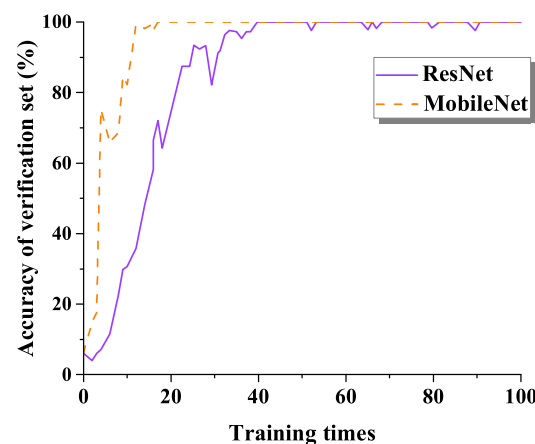**FIGURE 7.** Training process of convolutional neural network.



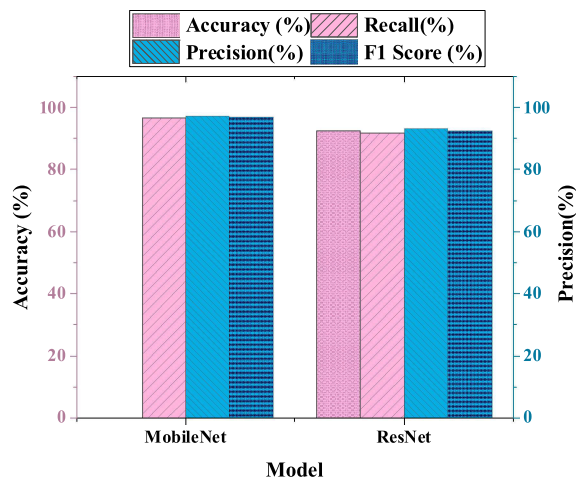**FIGURE 8.** The training process of Resnet and MobileNet models.



**FIGURE 9.** Performance test results of complex DL algorithm in human nutritional toxicology detection.

performance test results of the complex DL algorithm in human nutritional toxicology are given in Figure 9.

Figure 9 suggests that MobileNet outperforms other models in toxicology detection tasks, achieving higher accuracy

(96.8%), precision (97.2%), recall (96.5%), and F1 score (96.8%). These highlight the MobileNet model's suitability for toxicology detection in this particular task, delivering superior classification performance compared to ResNet. To provide a broader perspective, the performance of these four DL algorithms is compared with the two machine classification algorithms: Support Vector Machine (SVM) and Extreme Learning Machine (ELM), as portrayed in Figure 10.
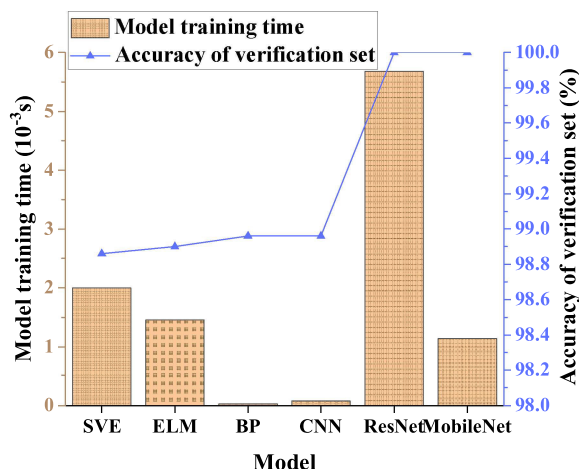


**FIGURE 10.** Comparison of six classification algorithms.

In Figure 10, concerning model training time, BPNN ($0.03 * 10^{-3}$ s) and CNN ($0.078 * 10^{-3}$ s) exhibit the shortest training duration, indicating their faster training speed. ResNet ($5.68 * 10^{-3}$ s) requires the most extended training time, followed by MobileNet ($1.14 * 10^{-3}$ s). The training time of SVE and ELM falls between the DL and the traditional ML models, though it is relatively short. The ResNet and MobileNet models achieve 100% accuracy regarding the validation set's accuracy, demonstrating their outstanding performance in toxicology detection tasks. BPNN and CNN are closely behind, with an accuracy of 98.96%. While slightly less accurate, SVE and ELM maintain accuracy levels above 98%. Considering the training time and accuracy, the MobileNet model balances computational speed and performance, showing swift training speed and high accuracy. In contrast, the ResNet model attains the highest accuracy but comes at the expense of a longer training duration.

Considering the practical feasibility of the new toxicological detection methods used in this study in BP, CNN, MobileNet, and ResNet models, the results of communication cost and calculation cost of different models in toxicological detection are detailed in Table 5. It can be observed that the BP and ResNet models are similar in communication cost, while the MobileNet model is relatively low. Regarding calculation cost, the BP and MobileNet models both show lower costs, while the CNN and ResNet models are higher. Considering the combination of communication cost and calculation cost, it can be found that the MobileNet model has a higher feasibility in toxicology detection. Because it shows relatively low communication and calculation costs.

**TABLE 5.** Communication cost and calculation cost results of different models in toxicology detection.

| Model | Communication cost (MB) | Calculation cost (s) |
|---|---|---|
| BP model | 120 | 0.8 |
| CNN model | 130 | 1.5 |
| MobileNet model | 100 | 0.5 |
| ResNet model | 120 | 1.2 |

**TABLE 6.** Results of cross-comparison between DL technology and traditional toxicological detection methods.

| Model | Detection time (min) | | | | | Substitutability | Prediction accuracy (%) |
|---|---|---|---|---|---|---|---|
| | A | B | C | D | E | - | - |
| BP model | 20 | 8 | 12 | 15 | 30 | Lower | 90 |
| CNN model | 15 | 6 | 10 | 12 | 25 | Higher | 89 |
| MobileNet model | 12 | 4 | 8 | 10 | 20 | High | 97 |
| ResNet model | 14 | 5 | 9 | 11 | 22 | High | 93 |

This indicates that the MobileNet model may have higher practical application potential and feasibility in toxicology detection.

To evaluate the time efficiency, substitutability, and predictive power of the toxicological detection method combined with THz technology and DL method used here, the traditional toxicological detection (animal experiment (A)/ in vitro test (B)/ chemical analysis (C)/ acute toxicity test (D)/ chronic toxicity test (E) is cross-compared with the used DL method. The analysis results are revealed in Table 6. It can be seen that compared with traditional toxicology detection methods, the BP model has the longest detection time. However, it still significantly reduces the detection time of traditional methods, and the prediction accuracy is maintained at a high level. The CNN and ResNet models are better than the BP model in terms of detection time, substitutability, and prediction accuracy, and their performance is stable. The MobileNet model presents excellent advantages in all aspects, with the shortest detection time, the highest prediction accuracy, and high fungibility, providing strong support for future toxicology research.

### D. DISCUSSION

In summary, the DL algorithm exhibits faster prediction times, improved stability, and greater accuracy when compared to ML. These study findings are further compared to those of prior research. For instance, Sujatha et al. evaluated the efficacy of six DL methods (Incident-V3, Visual Geometry Group (VGG)-16, and VGG-19) and three ML

algorithms (SVM, Random Forest (RF), and Random Gradient Descent) for the diagnosis of citrus plant diseases. They discovered that DL outperformed ML, with RF achieving the lowest disease classification accuracy, while VGG-16 demonstrated the highest accuracy (89.5). Their research also underscores the superiority of DL over ML, aligning with this study's results despite differences in application domains. To develop a system for detecting suicidal ideation, Aldhyani et al. employed a publicly accessible Reddit dataset, utilized the word embedding approach for text representation, and implemented a hybrid DL and ML algorithm for classification. CNN, a bidirectional LSTM model, and the ML XGBoost model were used to categorize suicidal or non-suicidal social posts. Their findings demonstrated that the bidirectional LSTM model outperformed the XGBoost model in the context of text-based characteristics, achieving a 95% accuracy in suicidal thought detection [41]. This result aligns with this study, reinforcing the superiority of DL algorithms. In the realm of medical imaging, Castiglioni et al. examined the distinctions between ML and DL. They provided an overview of the feature selection process via ML and the stages of training, verification, and testing. Furthermore, they highlighted DL's capability to process images directly, emphasizing the practical advantages of DL over ML methods [17].

Moreover, this study focuses on toxicological detection, presenting a new approach to improve public health and safety by combining DL and THz techniques. What sets this study apart from others is its unique amalgamation of DL technology and THz for identifying toxicants in health products. This innovative approach opens up new avenues in the field of toxicological detection. Furthermore, the experimental results clearly underscore the exceptional performance of the DL model in toxicological detection, surpassing the efficacy of conventional methods. Therefore, the study findings carry significant potential for practical applications promoting public health and safety.

Wang et al. used sparse principal component analysis to condense the features of drugs and proteins into a uniform carrier space. They also constructed a deep LSTM model for prediction, achieving an impressive area under the curve value of over 90% on drug target datasets. The research highlighted the potential of DL in drug discovery and development, particularly in predicting drug-protein interactions. While both studies leverage DL technology, they differ in terms of research subjects and objectives [47]. Similarly, Baptista et al. [10] employed DL methods to forecast drug response in cancer cell lines. Their findings demonstrated that the DL-based model performed on par with or even outperformed traditional ML models in predicting drug responses. While this study shares a commonality in applying DL to life sciences, it distinctly focuses on toxicological detection, diverging from Baptista et al.'s emphasis on cancer cell line drug responses. Sharma et al. adopted a DL framework to model in vitro and in vivo simultaneously and clinical toxicity data. They observed that viral were more closely correlated with in vitro (53%) and in vivo (56%) endpoints than with clinical data (8%) [22]. Their work delved into various facets of toxicity data, shedding light on differences between data endpoints and the preference of vector data for in vitro and in vivo experimental data. This comprehensive exploration proved valuable for understanding toxicity mechanisms and the effects of toxicants, echoing the potential of DL in toxicology research, as exemplified in this study.

## V. CONCLUSION

This study discusses the prospective application of DL technology in nutritional toxicology detection tasks. It uses four DL algorithms (BPNN, CNN, ResNet, and MobileNet) to scrutinize and predict potential toxicity in human nutrition. This leads to the following conclusions: (1) As training duration extends, model accuracy steadily improves. The final accuracy of BPNN and CNN culminates at 98.96%. Conversely, ResNet and MobileNet models attain a flawless 100% accuracy. (2) Among the four DL techniques, BPNN exhibits the swiftest prediction time, whereas the MobileNet model consistently secures the highest and most consistent accuracy. (3) The DL algorithm surpasses the ML algorithm regarding prediction speed, accuracy, and performance. Overall, the MobileNet model excels with excellent accuracy, precision, recall rate, and F1 score, establishing a superior classification performance compared to other models. (4) This study underscores the vast potential of DL technology for toxicology detection, offering a promising avenue for enhancing the safety of food and cosmetic products while mitigating potential risks. It underscores the pivotal role of DL in augmenting public health and safety in this context.

However, this study bears certain limitations that warrant acknowledgment. Firstly, despite utilizing a more extensive and diverse dataset, potential sample bias remains, potentially impacting the model's generalization abilities. Secondly, this study mainly focuses on the comparative performance comparison of four DL algorithms. While these algorithms have seen enhancements, the quest for improved accuracy in toxicology detection remains an ongoing challenge. Furthermore, this study could be broadened to a broader array of chemicals and food products to yield a more comprehensive spectrum of research outcomes. Future research should encompass the refinement of the DL model to enhance its efficacy in toxicological detection, while simultaneously considering integrating additional data sources and innovative feature engineering methods. Moreover, exploring advanced DL architectures is a promising avenue to elevate the model's classification performance. Finally, this study's methodology could be readily applied to real-world product safety assessment to ensure the quality and safety of items such as food and cosmetics.

## REFERENCES

[1] A. Kumari and S. Tanwar, "Reveal: An AI-based big data analytics scheme for energy price prediction and load reduction," in *Proc. 11th Int. Conf. Cloud Comput., Data Sci. Eng. (Confluence)*, Jan. 2021, pp. 321–326.

[2] A. Kumari, D. Vekaria, R. Gupta, and S. Tanwar, "Redills: Deep learning-based secure data analytic framework for smart grid systems," in *Proc. IEEE Int. Conf. Commun. Workshops (ICC Workshops)*, Jun. 2020, pp. 1–6.

[3] A. Kumari, S. Tanwar, S. Tyagi, and N. Kumar, "Verification and validation techniques for streaming big data analytics in Internet of Things environment," *IET Netw.*, vol. 8, no. 3, pp. 155–163, May 2019.

[4] A. Kumari, S. Tanwar, S. Tyagi, and N. Kumar, "Fog computing for healthcare 4.0 environment: Opportunities and challenges," *Comput. Electr. Eng.*, vol. 72, pp. 1–13, Nov. 2018.

[5] A. Kumari, S. Tanwar, S. Tyagi, N. Kumar, M. Maasberg, and K.-K.-R. Choo, "Multimedia big data computing and Internet of Things applications: A taxonomy and process model," *J. Netw. Comput. Appl.*, vol. 124, pp. 169–195, Dec. 2018.

[6] A. Nawaz, X. Su, Q. M. U. Din, M. I. Khalid, M. Bilal, and S. A. R. Shah, "Identification of the H&S (health and safety factors) involved in infrastructure projects in developing countries—A sequential mixed method approach of OLMT-project," *Int. J. Environ. Res. Public Health*, vol. 17, no. 2, p. 635, Jan. 2020.

[7] A. Paul, V. N. Dhamu, S. Muthukumar, and S. Prasad, "EPASS: Electroanalytical pillbox assessment sensor system, a case study using metformin hydrochloride," *Anal. Chem.*, vol. 94, no. 30, pp. 10617–10625, Aug. 2022.

[8] B. Sharma, V. Chenthamarakshan, A. Dhurandhar, S. Pereira, J. A. Hendler, J. S. Dordick, and P. Das, "Accurate clinical toxicity prediction using multi-task deep neural nets and contrastive molecular explanations," *Sci. Rep.*, vol. 13, no. 1, p. 4908, Mar. 2023.

[9] C. Han, Y. Wang, Y. Li, Y. Chen, N. A. Abbasi, T. Kürner, and A. F. Molisch, "Terahertz wireless channels: A holistic survey on measurement, modeling, and analysis," *IEEE Commun. Surveys Tuts.*, vol. 24, no. 3, pp. 1670–1707, 3rd Quart., 2022.

[10] C. Kooli, "COVID-19: Public health issues and ethical dilemmas," *Ethics, Med. Public Health*, vol. 17, Jun. 2021, Art. no. 100635.

[11] D. Baptista, P. G. Ferreira, and M. Rocha, "Deep learning for drug response prediction in cancer," *Briefings Bioinf.*, vol. 22, no. 1, pp. 360–379, Jan. 2021.

[12] D. C. Filipoiu, S. G. Bungau, L. Endres, P. A. Negru, A. F. Bungau, B. Pasca, A.-F. Radu, A. G. Tarce, M. A. Bogdan, T. Behl, A. C. Nechifor, S. S. U. Hassan, and D. M. Tit, "Characterization of the toxicological impact of heavy metals on human health in conjunction with modern analytical methods," *Toxics*, vol. 10, no. 12, p. 716, Nov. 2022.

[13] D. Fan, Y. Li, W. Liu, X.-G. Yue, and G. Boustras, "Weaving public health and safety nets to respond the COVID-19 pandemic," *Saf. Sci.*, vol. 134, Feb. 2021, Art. no. 105058.

[14] D. Qiu, L. Zheng, J. Zhu, and D. Huang, "Multiple improved residual networks for medical image super-resolution," *Future Gener. Comput. Syst.*, vol. 116, pp. 200–208, Mar. 2021.

[15] D. R. Sarvamangala and R. V. Kulkarni, "Convolutional neural networks in medical image understanding: A survey," *Evol. Intell.*, vol. 15, no. 1, pp. 1–22, Mar. 2022.

[16] D. Vekaria, A. Kumari, S. Tanwar, and N. Kumar, "Boost: An AI-based data analytics scheme for COVID-19 prediction and economy boosting," *IEEE Internet Things J.*, vol. 8, no. 21, pp. 15977–15989, Nov. 2021.

[17] E. F. Boadu, C. C. Wang, and R. Y. Sunindijo, "Characteristics of the construction industry in developing countries and its implications for health and safety: An exploratory study in Ghana," *Int. J. Environ. Res. Public Health*, vol. 17, no. 11, p. 4110, Jun. 2020.

[18] I. Castiglioni, L. Rundo, M. Codari, G. Di Leo, C. Salvatore, M. Interlenghi, F. Gallivanone, A. Cozzi, N. C. D'Amico, and F. Sardanelli, "AI applications to medical images: From machine learning to deep learning," *Phys. Medica*, vol. 83, pp. 9–24, Mar. 2021.

[19] I. F. Akyildiz, C. Han, Z. Hu, S. Nie, and J. M. Jornet, "Terahertz band communication: An old problem revisited and research directions for the next decade," *IEEE Trans. Commun.*, vol. 70, no. 6, pp. 4250–4285, Jun. 2022.

[20] J. Lietzow, "Biologically active compounds in mustard seeds: A toxicological perspective," *Foods*, vol. 10, no. 9, p. 2089, Sep. 2021.

[21] K. Abbas, M. Afaq, T. A. Khan, and W.-C. Song, "A blockchain and machine learning-based drug supply chain management and recommendation system for smart pharmaceutical industry," *Electronics*, vol. 9, no. 5, p. 852, May 2020.

[22] L. Wang, Y. Cheng, W. Wang, J. Zhao, Y. Wang, X. Zhang, M. Wang, T. Shan, and M. He, "Effects of terahertz radiation on the aggregation of Alzheimer's A$\beta$42 peptide," *Int. J. Mol. Sci.*, vol. 24, no. 5, p. 5039, Mar. 2023.

[23] L. Wu, B. Yan, J. Han, R. Li, J. Xiao, S. He, and X. Bo, "TOXRIC: A comprehensive database of toxicological data and benchmarks," *Nucleic Acids Res.*, vol. 51, no. D1, pp. D1432–D1445, Jan. 2023.

[24] L. Zhao, H. L. Ciallella, L. M. Aleksunes, and H. Zhu, "Advancing computer-aided drug discovery (CADD) by big data and data-driven machine learning modeling," *Drug Discovery Today*, vol. 25, no. 9, pp. 1624–1638, Sep. 2020.

[25] M. Raghu, T. Unterthiner, S. Kornblith, C. Zhang, and A. Dosovitskiy, "Do vision transformers see like convolutional neural networks?" in *Proc. Adv. Neural Inf. Process. Systems.*, vol. 34, 2021, pp. 12116–12128.

[26] P. Kiran, B. D. Parameshachari, J. Yashwanth, and K. N. Bharath, "Offline signature recognition using image processing techniques and back propagation neuron network system," *Social Netw. Comput. Sci.*, vol. 2, no. 3, pp. 1–8, May 2021.

[27] P. N. Srinivasu, J. G. Sivasai, M. F. Ijaz, A. K. Bhoi, W. Kim, and J. J. Kang, "Classification of skin disease using deep learning neural networks with MobileNet v2 and LSTM," *Sensors*, vol. 21, no. 8, p. 2852, Apr. 2021.

[28] P. Wang, E. Fan, and P. Wang, "Comparative analysis of image classification algorithms based on traditional machine learning and deep learning," *Pattern Recognit. Lett.*, vol. 141, pp. 61–67, Jan. 2021.

[29] Q. Zhao, H. Zhao, K. Zheng, and J. Wang, "HyperAttentionDTI: Improving drug–protein interaction prediction by sequence-based deep learning with attention mechanism," *Bioinformatics*, vol. 38, no. 3, pp. 655–662, Jan. 2022.

[30] R. Pratiwi, R. H. F. Dipadharma, I. J. Prayugo, and O. A. Layandro, "Recent analytical method for detection of chemical adulterants in herbal medicine," *Molecules*, vol. 26, no. 21, p. 6606, Oct. 2021.

[31] R. Sujatha, J. M. Chatterjee, N. Jhanjhi, and S. N. Brohi, "Performance of deep learning vs machine learning in plant leaf disease detection," *Microprocessors Microsyst.*, vol. 80, Feb. 2021, Art. no. 103615.

[32] S. Bouguezzi, H. B. Fredj, T. Belabed, C. Valderrama, H. Faiedh, and C. Souani, "An efficient FPGA-based convolutional neural network for classification: Ad-MobileNet," *Electronics*, vol. 10, no. 18, p. 2272, Sep. 2021.

[33] S. C. Moyce and M. Schenker, "Migrant workers and their occupational health and safety," *Annu. Rev. Public Health*, vol. 39, no. 1, pp. 351–365, Apr. 2018.

[34] S. Kiranyaz, O. Avci, O. Abdeljaber, T. Ince, M. Gabbouj, and D. J. Inman, "1D convolutional neural networks and applications: A survey," *Mech. Syst. Signal Process.*, vol. 151, Apr. 2021, Art. no. 107398.

[35] S. Lake, T. Kerr, D. Werb, R. Haines-Saah, B. Fischer, G. Thomas, Z. Walsh, M. A. Ware, E. Wood, and M. Milloy, "Guidelines for public health and safety metrics to evaluate the potential harms and benefits of cannabis regulation in Canada," *Drug Alcohol Rev.*, vol. 38, no. 6, pp. 606–621, Sep. 2019.

[36] S. M. Campbell and J. Rosen, "The intersectionality of activism and public health in new York state: Can labor/health and safety move addiction recovery forward?" *New Solutions, J. Environ. Occupational Health Policy*, vol. 31, no. 3, pp. 330–339, Nov. 2021.

[37] S. Nag, A. T. K. Baidya, A. Mandal, A. T. Mathew, B. Das, B. Devi, and R. Kumar, "Deep learning tools for advancing drug discovery and development," *3 Biotech*, vol. 12, no. 5, p. 110, May 2022.

[38] S. Rodriguez, C. Hug, P. Todorov, N. Moret, S. A. Boswell, K. Evans, G. Zhou, N. T. Johnson, B. T. Hyman, and P. K. Sorger, "Machine learning identifies candidates for drug repurposing in Alzheimer's disease," *Nature Commun.*, vol. 12, no. 1, p. 1033, 2021.

[39] S. Tanwar, A. Kumari, D. Vekaria, M. S. Raboaca, F. Alqahtani, A. Tolba, B.-C. Neagu, and R. Sharma, "GrAb: A deep learning-based data-driven analytics scheme for energy theft detection," *Sensors*, vol. 22, no. 11, p. 4048, May 2022.

[40] S. Tanwar, A. Kumari, D. Vekaria, N. Kumar, and R. Sharma, "An AI-based disease detection and prevention scheme for COVID-19," *Comput. Electr. Eng.*, vol. 103, Oct. 2022, Art. no. 108352.

[41] T. Gouin, R. Ellis-Hutchings, L. M. Thornton Hampton, C. L. Lemieux, and S. L. Wright, "Screening and prioritization of nano- and microplastic particle toxicity studies for evaluating human health risks—Development and application of a toxicity study assessment tool," *Microplastics Nanoplastics*, vol. 2, no. 1, p. 2, Jan. 2022.

[42] T. H. H. Aldhyani, S. N. Alsubari, A. S. Alshebami, H. Alkahtani, and Z. A. T. Ahmed, "Detecting and analyzing suicidal ideation on social media using deep learning and machine learning models," *Int. J. Environ. Res. Public Health*, vol. 19, no. 19, p. 12635, Oct. 2022.

[43] T. O'Leary-Roseberry, X. Du, A. Chaudhuri, J. R. R. A. Martins, K. Willcox, and O. Ghattas, "Learning high-dimensional parametric maps via reduced basis adaptive residual networks," *Comput. Methods Appl. Mech. Eng.*, vol. 402, Dec. 2022, Art. no. 115730.

[44] U. Kulkarni, S. M. Meena, S. V. Gurlahosur, and G. Bhogar, "Quantization friendly MobileNet (QF-MobileNet) architecture for vision based applications on embedded platforms," *Neural Netw.*, vol. 136, pp. 28–39, Apr. 2021.

[45] V. Safonov, "Assessment of heavy metals in milk produced by black-and-White Holstein cows from Moscow," *Current Res. Nutrition Food Sci. J.*, vol. 8, no. 2, pp. 410–415, Aug. 2020.

[46] Y. Deng, X. Zhou, J. Shen, G. Xiao, H. Hong, H. Lin, F. Wu, and B.-Q. Liao, "New methods based on back propagation (BP) and radial basis function (RBF) artificial neural networks (ANNs) for predicting the occurrence of haloketones in tap water," *Sci. Total Environ.*, vol. 772, Jun. 2021, Art. no. 145534.

[47] Y. Pan, "The influence of Ag and Cu on the electronic and optical properties of ZrO from first-principles calculations," *Mater. Sci. Semicond. Process.*, vol. 135, Nov. 2021, Art. no. 106084.

[48] Y.-B. Wang, Z.-H. You, S. Yang, H.-C. Yi, Z.-H. Chen, and K. Zheng, "A deep learning-based method for drug-target interaction prediction based on long short-term memory neural network," *BMC Med. Informat. Decis. Making*, vol. 20, no. S2, pp. 1–9, Mar. 2020.

[49] Z. Li, F. Liu, W. Yang, S. Peng, and J. Zhou, "A survey of convolutional neural networks: Analysis, applications, and prospects," *IEEE Trans. Neural Netw. Learn. Syst.*, vol. 33, no. 12, pp. 6999–7019, Dec. 2022.

[50] Z. Zheng, Y. Zheng, Y. Luo, Z. Yi, J. Zhang, Z. Liu, W. Yang, Y. Yu, X. Wu, and P. Wu, "A switchable terahertz device combining ultra-wideband absorption and ultra-wideband complete reflection," *Phys. Chem. Chem. Phys.*, vol. 24, no. 4, pp. 2527–2533, 2022.

• • •